⌘ *Author's Choice*

THE JOURNAL OF BIOLOGICAL CHEMISTRY VOL. 288, NO. 11, pp. 7803–7814, March 15, 2013

Structural Basis for Cul3 Protein Assembly with the BTB-Kelch Family of E3 Ubiquitin Ligases*[S]

Received for publication, November 19, 2012, and in revised form, January 7, 2013 Published, JBC Papers in Press, January 24, 2013, DOI 10.1074/jbc.M112.437996

Peter Canning, Christopher D. O. Cooper, Tobias Krojer, James W. Murray[1], Ashley C. W. Pike, Apirat Chaikuad, Tracy Keates, Chancievan Thangaratnarajah, Viktorija Hojzan, Brian D. Marsden, Opher Gileadi, Stefan Knapp, Frank von Delft, and Alex N. Bullock[2]

From the Structural Genomics Consortium, University of Oxford, Oxford OX3 7DQ, United Kingdom

Background: BTB-Kelch proteins, including KLHL11, are proposed to bind Cul3 through a "3-box" motif to form E3 ubiquitin ligases.
Results: We solved crystal structures of the KLHL11-Cul3 complex and four Kelch domains.
Conclusion: The 3-box forms a hydrophobic groove that binds a specific N-terminal extension of Cul3.
Significance: Dimeric BTB-Kelch proteins bind two Cul3 molecules and support a two-site model for substrate recognition.

Cullin-RING ligases are multisubunit E3 ubiquitin ligases that recruit substrate-specific adaptors to catalyze protein ubiquitylation. Cul3-based Cullin-RING ligases are uniquely associated with BTB adaptors that incorporate homodimerization, Cul3 assembly, and substrate recognition into a single multidomain protein, of which the best known are BTB-BACK-Kelch domain proteins, including KEAP1. Cul3 assembly requires a BTB protein "3-box" motif, analogous to the F-box and SOCS box motifs of other Cullin-based E3s. To define the molecular basis for this assembly and the overall architecture of the E3, we determined the crystal structures of the BTB-BACK domains of KLHL11 both alone and in complex with Cul3, along with the Kelch domain structures of KLHL2 (Mayven), KLHL7, KLHL12, and KBTBD5. We show that Cul3 interaction is dependent on a unique N-terminal extension sequence that packs against the 3-box in a hydrophobic groove centrally located between the BTB and BACK domains. Deletion of this N-terminal region results in a 30-fold loss in affinity. The presented data offer a model for the quaternary assembly of this E3 class that supports the bivalent capture of Nrf2 and reveals potential new sites for E3 inhibitor design.

Ubiquitylation proceeds through a cascade of enzymatic reactions catalyzed by the E1, E2, and E3 enzymes (1, 2). The E1 ubiquitin-activating enzyme uses ATP to catalyze the covalent transfer of ubiquitin to the active site cysteine of an E2 ubiquitin-conjugating enzyme. An E3 ubiquitin ligase further catalyzes the transfer of ubiquitin from the E2 to a substrate lysine. Cullin-RING ligases (CRLs)[3] are the largest family of multisubunit E3 ubiquitin ligases and adopt a modular assembly that facilitates the ubiquitylation of divergent substrates. The Cullin subunit (Cul1–5 or Cul7) forms a central stalk-like scaffold that orients and constrains the substrate binding and catalytic centers (3, 4). The N-terminal domain (NTD) binds a specific substrate-recognition domain, usually through an adaptor protein, whereas the C-terminal domain (CTD) binds a RING (Really Interesting New Gene) protein (Rbx1 or Rbx2), which in turn recruits an E2-ubiquitin conjugate. Neddylation of the CTD is additionally required to induce conformational changes in the CRL that bring the substrate and E2-ubiquitin into juxtaposition (5, 6). The crystal structure of an entire CRL1 complex (also known as a SCF (Skp1-Cul1-F-box) E3 ligase) (7) suggests that different CRLs confer different spacings to allow substrates of varying sizes to be ubiquitylated.

The CRL3 subclass utilizes Cul3, which combines exclusively with BTB-containing proteins as substrate-specific adaptors (8). The BTB domain (Bric-a-brac, Tramtrack, and Broad complex), first characterized by the crystal structure of the promyelocytic leukemia zinc finger protein (9), shares a conserved fold with the Cul1 adaptor Skp1 (10) and the Cul2/5 adaptor ElonginC (11). Moreover, the structure of the SPOP BTB domain in complex with the $Cul3_{NTD}$ shows an assembly similar to the CRL1 complex of Skp1 and Cul1 (12). However, two features make the BTB adaptors unique among CRLs. First, the BTB adaptor domain dimerizes and is therefore capable of recruiting two Cul3 subunits into the CRL3 complex. Second, the BTB-containing proteins typically host a second protein-protein interaction domain, so that a single subunit functions as both adaptor and substrate-recognition module. The latter include the C-terminal Kelch, PHR (PAM, Highwire, and RPM-1), or zinc finger domains, whereas SPOP contains an N-terminal MATH (meprin and TRAF homology) domain (13).

* The Structural Genomics Consortium is a registered charity (number 1097737) that receives funds from the Canadian Institutes for Health Research, Genome Canada, GlaxoSmithKline, Lilly Canada, the Novartis Research Foundation, Pfizer, Takeda, AbbVie, the Canada Foundation for Innovation, the Ontario Ministry of Economic Development and Innovation, and Wellcome Trust Grant 092809/Z/10/Z.
⌘ *Author's Choice*—Final version full access.
[S] This article contains supplemental Fig. S1, Table S1, and an additional reference.
The atomic coordinates and structure factors (codes 2VPJ, 2XN4, 3II7, 3I3N, 4APF, 4AP2, and 4ASC) have been deposited in the Protein Data Bank (http://wwpdb.org/).
[1] Present address: Dept. of Life Sciences, Imperial College, Exhibition Road, London SW7 2AZ, UK.
[2] To whom correspondence should be addressed. Tel.: 44-1865-617754; Fax: 44-1865-617575; E-mail: alex.bullock@sgc.ox.ac.uk.

[3] The abbreviations used are: CRL, Cullin-RING ligase; ITC, isothermal titration calorimetry; NTD, N-terminal domain; CTD, C-terminal domain; BTB, Bric-a-brac, Tramtrack, and Broad complex.

The most common substrate-recognition domain in the CRL3 subclass is the Kelch β-propeller domain (14), which occurs C-terminal to BTB and BACK (for BTB and C-terminal Kelch") domains (15). The best known example of a BTB-Kelch protein is KEAP1, which associates with Cul3 to regulate cellular levels of the transcription factor Nrf2, a master regulator of the anti-oxidant response (16, 17). KEAP1 demonstrates how important the dimeric CRL3 architecture is for substrate ubiquitylation as it requires two Kelch domains to engage two distinct epitopes in Nrf2 simultaneously (18–21). KEAP1 mutations that disrupt Nrf2 ubiquitylation are associated with lung cancer progression and chemoresistance (22, 23). Mutations in the BTB-Kelch proteins KLHL3, KLHL7, and KLHL9 are additionally associated with hypertension (24), retinitis pigmentosa (25), and distal myopathy (26), respectively, although their corresponding substrates have yet to be identified. After KEAP1, the best characterized protein is KLHL12, which modulates COPII assembly for collagen export (27) and also ubiquitylates both the dopamine D4 receptor (28) and dishevelled (29).

Recent structures of SPOP-substrate complexes identify a two-helix extension of the BTB domain that is critical for high affinity Cul3 interaction (30). Defined as the "3-box," this motif appears common to all BTB adaptor proteins (30). To understand the molecular basis for this assembly and to establish structural models for the dimeric BTB-Kelch family, we determined the crystal structures of the BTB-BACK domains of KLHL11 both alone and in complex with Cul3, along with the structures of four representative Kelch domains. The presented data provide a structural model for the understanding of the specific assembly of the BTB-Kelch E3 adaptor proteins with Cul3.

EXPERIMENTAL PROCEDURES

Protein Expression and Purification—Human KLHL11 (UniProt Q9NVR0, residues 67–340), KLHL2 (O95198, residues 294–593), KLHL7 (Q8IXQ5, residues 283–586), and KLHL12 (Q53G59, residues 268–567) were subcloned into the vector pNIC28-Bsa4. Human $Cul1_{NTD}$ (Q13616, residues 1–412), $Cul3_{NTD}$ (Q13618, residues 1–390), $Cul3_{NTD\Delta N22}$ (residues 23–390), $Cul5_{NTD}$ (Q93034, residues 1–386), and KBTBD5 (Q2TBA0, residues 314–621) were subcloned into the vector pNIC-CTHF using ligation-independent cloning, as described previously (31). Two point mutations were introduced into the Cul1 (V367R and L371D), Cul3 (I342R and L346D), and Cul5 (V341R and L345D) sequences to stabilize the isolated N-terminal domains. Proteins were expressed in BL21(DE3)-R3-pRARE cells using 0.5 mM isopropyl 1-thio-β-D-galactopyranoside for overnight induction at 18 °C. Harvested cells were resuspended in binding buffer (50 mM HEPES, pH 7.5, 500 mM NaCl, 5% glycerol, 5 mM imidazole) supplemented with 1 mM phenylmethylsulfonyl fluoride and 1 mM tris(2-carboxyethyl)-phosphine and disrupted by sonication or high pressure homogenization. Proteins were purified by nickel affinity and size exclusion chromatography (proteins for complexes were mixed 1:1 after IMAC). A final ion exchange step was used for KLHL7 (Mono S) and the KLHL11-Cul3 complexes (HiTrap Q). Tobacco etch virus protease A was used to cleave the polyhistidine tags from KLHL2, KLHL7, KLHL12, and KBTBD5 overnight at 4 °C. Selenomethionine-substituted KLHL11 was prepared using M9 minimal growth media supplemented with selenomethionine during the exponential growth phase.

Crystallization and Data Collection—Crystals were grown using the sitting-drop vapor-diffusion technique and cryoprotected before being vitrified in liquid nitrogen (full conditions are listed in Table 1). Diffraction experiments were conducted at 100 K. Data were collected using synchrotron radiation with the exception of KLHL7, for which a full dataset was collected using a Rigaku FR-E SuperBright rotating-anode x-ray generator. Crystallographic data are provided in Table 2. To calculate experimental phases, datasets were collected from crystals of selenomethionine-substituted KLHL11 at a wavelength of 0.9794 Å and from crystals of the KLHL11-$Cul3_{NTD\Delta N22}$ complex soaked with 2 mM thimerosal at a wavelength of 0.9686 Å.

Structure Determination—Data were integrated using Mosflm (32) or XDS (33) and scaled with SCALA (34) or AIMLESS as part of the CCP4 software suite (35). Experimental phases were calculated, and density modification was carried out with autoSHARP (36). Alternatively, phases were calculated using molecular replacement with PHASER (37) and density modification conducted with PARROT (38). Automated model building tasks were conducted with BUCCANEER (39, 40) or PHENIX.AUTOBUILD (41). Manual model building was performed with COOT (42) and the models refined with CNS (43, 44), REFMAC (45, 46), or BUSTER (47) using TLS and NCS restraints as appropriate. Experimental phase restraints were included in the refinement of the KLHL11-$Cul3_{NTD\Delta N22}$ complex until the final round of refinement. The model of this Cul3 complex was used as a molecular replacement solution for the higher resolution KLHL11-$Cul3_{NTD}$ structure. The final model was completed manually and refined to completion. Models were validated using the PHENIX (41) validation tools and/or MOLPROBITY (48).

Isothermal Titration Calorimetry—ITC experiments were performed at 15 °C using a Microcal VP-ITC microcalorimeter. Proteins were dialyzed into a buffer containing 50 mM HEPES, pH 7.5, 150 mM NaCl, 0.5 mM tris(2-carboxyethyl)phosphine. Cullin proteins (90–125 μM) were titrated into KLHL11 (10 μM). Data were analyzed using a single binding site model implemented in the Origin software package provided with the instrument.

RESULTS

BTB-Kelch Family—The human genome contains some 52 BTB-Kelch family proteins (Fig. 1 and supplemental Table S1). Their nomenclature is varied, but the protein family can be subdivided into the Kelch-like (KLHL(1–39)) and the Kelch repeat and BTB domain-containing proteins (KBTBD(1–13)). To derive structural models for their function as Cul3-based E3 ligases, members of this family were subcloned and screened for bacterial expression. Soluble expression constructs were identified that contained the BTB-BACK or Kelch domains but not the BACK-Kelch or BTB-BACK-Kelch domains. Crystal structures of the BTB-BACK domains of human KLHL11 were subsequently solved alone and in complex with the N-terminal Cullin-repeat domain of Cul3. Additional structures were solved of the Kelch domains of human KLHL2 (Mayven), KLHL7, KLHL12, and KBTBD5 (see Table 1 for crystallization

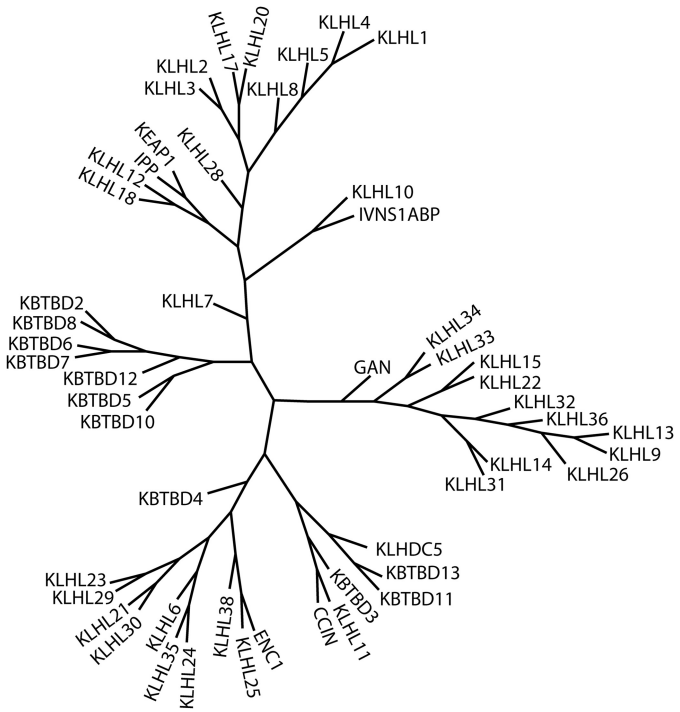

FIGURE 1. **Phylogenetic tree of human Kelch domains from the BTB-Kelch family.** *A*, multiple sequence alignment of human Kelch domains was generated using ClustalX (version 1.83) (65) and manually refined with reference to publicly available structures. A phylogenetic tree was created from this alignment using the N-J Tree export functionality of ClustalX and a radial tree figure prepared in PhyloDraw (version 0.8) (66). Further descriptions of each protein are given in supplemental Table S1.

conditions). A summary of statistics for data collection and refinement is reported in Table 2.

Structure of the BTB-BACK Domains of KLHL11—The structure of the BTB-BACK domains of KLHL11 (Fig. 2*A*, residues 67–340) was determined at 2.6-Å resolution using phases calculated from single-wavelength anomalous diffraction collected from selenomethionine-incorporated protein crystals. Two protein chains were present in the asymmetric unit forming a homodimer with an elongated shape of overall dimensions 150 × 35 × 25 Å (Fig. 2*B*). The BTB domain of KLHL11 closely resembles the common BTB fold of promyelocytic leukemia zinc finger protein (PDB code 1BUO, root mean square deviation 4.65 Å for 118 Cα atoms) (9). An interchain $\beta1-\beta5'$ antiparallel β-sheet establishes the typical domain-swapped dimer, which is additionally stabilized by the interactions between helices $\alpha1$ and $\alpha2'$ (where ′ denotes the second chain) (Fig. 2*C*).

Portions of the all α-helical BACK domain, also known as the intervening region, have been previously structurally determined for Gigaxonin (KLHL16) (30) and KBTBD4 (PDB code 2EQX). KLHL11 is the first structure to span the entire domain and contains eight helices in total. The two N-terminal helices (KLHL11 $\alpha7-\alpha8$) make up the 3-box motif and bind helices $\alpha5$ and $\alpha6$ of the BTB domain in an antiparallel four helix bundle configuration (Fig. 2*C*). Significantly for Cul3 recognition, all three structures are closely conserved despite limited sequence identity. The remaining C-terminal helices $\alpha9-\alpha14$ form a distinct subdomain, packing perpendicular to the 3-box. Notably, this arrangement creates a significant cleft some 16 Å deep and

TABLE 1
Crystallization conditions
TCEP is tris(2-carboxyethyl)phosphine; Bistris propane is 1,3-bis[tris(hydroxymethyl)methylamino]propane; SeMet is selenomethionine.

	$KLHL11_{BTBBACK}$ + $CUL3_{NTD}$	$KLHL11_{BTBBACK}$ + $CUL3_{NTDΔN22}$	Hg-$KLHL11_{BTBBACK}$ + $CUL3_{NTDΔN22}$	$KLHL11_{BTBBACK}$	SeMet-$KLHL11_{BTBBACK}$	$KLHL2_{KELCH}$	$KLHL7_{KELCH}$	$KLHL12_{KELCH}$	$KBTBD5_{KELCH}$
Protein buffer	10 mM HEPES, pH 7.5, 150 mM NaCl, 0.5 mM TCEP	10 mM HEPES, pH 7.5, 150 mM NaCl, 1 mM TCEP	10 mM HEPES, pH 7.5, 150 mM NaCl, 1 mM TCEP	10 mM HEPES, pH 7.5, 500 mM NaCl, 5% glycerol	10 mM HEPES, pH 7.5, 500 mM NaCl, 5% glycerol	50 mM HEPES, pH 7.5, 500 mM NaCl, 5% glycerol, 0.5 mM TCEP	50 mM HEPES, pH 7.5, 100 mM NaCl, 10 mM DTT	50 mM HEPES, pH 7.5, 250 mM NaCl, 0.5 mM TCEP	50 mM HEPES, pH 7.5, 120 mM NaCl, 10 mM DTT, 10 mM Arg, 10 mM Glu
Concentration	8.5 mg/ml	7.5 mg/ml	7.5 mg/ml	6 mg/ml	6 mg/ml	8.85 mg/ml	10.1 mg/ml	8.9 mg/ml	11 mg/ml
Reservoir solution	0.1 M Bistris propane, pH 7, 25% PEG 3350, 0.15 M NaI, 8% ethylene glycol	0.1 M Bistris propane, pH 6.5, 0.25 M sodium malonate pH 7, 10% PEG 3350, 5% ethylene glycol	0.1 M Bistris propane, pH 6.5, 0.12 M potassium citrate, 17% PEG 3350, 10% ethylene glycol	0.1 M Bistris propane, pH 7.5, 0.25 M potassium thiocyanate, 25% PEG 3350, 5% ethylene glycol	0.1 M Bistris propane, pH 7.5, 0.25 M potassium thiocyanate, 25% PEG 3350, 5% ethylene glycol	0.2 M ammonium sulfate, 0.1 M MES, pH 6.5, 30% PEG 5K MME, 0.2 M sodium thiocyanate	0.1 M MES, pH 6.5, 12% PEG 20K	0.2 M ammonium acetate, 0.1 M sodium acetate pH 4.6, 30% PEG 4K	0.1 M citrate pH 5.3, 20% PEG 6K
Drop volume	300 nl	300 nl	450 nl	150 nl	150 nl	150 nl	150 nl	150 nl	150 nl
Protein: reservoir ratio	1:1	2:1	2:1	2:1	2:1	1:2	1:2	1:1	2:1
Temperature	20 °C	4 °C	4 °C	4 °C	4 °C	20 °C	20 °C	20 °C	4 °C
Cryoprotectant	25% ethylene glycol	25% ethylene glycol	25% ethylene glycol	25% ethylene glycol	25% ethylene glycol	25% ethylene glycol	30% ethylene glycol	15% PEG 400	25% ethylene glycol

TABLE 2

Crystallographic data collection and refinement statistics

ASU, asymmetric unit; r.m.s.d., root mean square deviation.

	$KLHL11_{BTBBACK}$ + $CUL3_{NTD}$	$KLHL11_{BTBBACK}$ + $Cul3_{NTD\Delta N22}$	Hg-$KLHL11_{BTBBACK}$ + $CUL3_{NTD\Delta N22}$	$KLHL11_{BTBBACK}$	SeMet-$KLHL11_{BTBBACK}$	$KLHL2_{KELCH}$	$KLHL7_{KELCH}$	$KLHL12_{KELCH}$	$KBTBD5_{KELCH}$
Data collection									
Beamline	Diamond I03	Diamond I02	Diamond I02	SLS-X10	SLS-X10	Diamond I24	In-house	SLS-X10	Diamond I04–1
Space group	*I*121	*C*121	*C*121	$P12_11$	$P12_11$	*P*1	*C*121	$P12_11$	$P2_12_12_1$
Cell dimensions									
a/*b*/*c*	147.5/40.2/234.8 Å	238.6/41.4/147.8 Å	148.5/42.4/233.4 Å	41.1/68.9/136.8 Å	41.2/68.7/135.5 Å	46.0/46.0/71.8 Å	76.4/50.9/87.5 Å	44.6/61.5/45.5 Å	61.3/65.0/89.2 Å
α/β/γ	90/107.3/90°	90/110.2/90°	90/105.1/90°	90/97.4/90°	90/96.7/90°	86.7/82.8/68.5°	90/113.2/90°	90/111.8/90°	90/90/90°
Resolution[a]	2.8 Å (2.95–2.8 Å)	3.1 Å (3.27–3.1 Å)	3.5 Å (3.69–3.5 Å)	2.6 Å (2.69–2.6 Å)	2.34 Å (2.46–2.34 Å)	1.99 Å (2.09–1.99 Å)	1.63 Å (1.67–1.63 Å)	1.85 Å (1.9–1.85 Å)	1.78 Å (1.82–1.78 Å)
Unique observations[a]	33,319 (4803)	25,043 (3523)	14,711 (293)	23,589 (3369)	28,166 (1786)	34,329 (3487)	38,407 (5515)	19,527 (2739)	34,642 (13,454)
Completeness[a]	100% (100%)	95.5% (96.8%)	80.4% (10.8%)	99.6% (98.2%)	87.8% (38.7%)	92.5% (67.8)	99.2% (98.8%)	99.4% (96.1%)	99.9% (99.9%)
Redundancy[a]	9 (9.2)	2.8 (2.8)	6.3 (1.3)	6.2 (4.7)	6.9 (2.2)	3.1 (2.4)	6.5 (6)	4.3 (3.4)	6.2 (6.4)
R_{merge}[a]	0.11 (1.12)	0.06 (0.5)	0.119 (0.727)	0.115 (0.492)	0.106 (0.575)	0.1 (0.32)	0.083 (0.0636	0.09 (0.63)	0.07 (0.56)
$I/\sigma I$[a]	12.2 (2.2)	9.8 (2.1)	9.2 (1)	13.3 (3.1)	12.7 (0.8)	8.9 (4.3)	13.8 (2.6)	10.6 (2)	13.9 (3.1)
Refinement									
Resolution	2.8 Å	3. Å 1		2.6 Å		1.99 Å	1.63 Å	1.85 Å	1.78 Å
MR model						3ADE	2VPJ	2DYH	2WOZ
Copies in ASU	1	1	1	2	2	2	1	1	1
R_{work}/R_{free}	20.4/23.6%	19.3/22.1%		26.0/28.6%		16.9/22.2%	16.1/19.0%	16.1/22.2%	17.8/22.6%
No. of atoms									
Protein	4758	4631		4364		4320	2310	2190	2395
Hetatoms	18			6		40	100	8	8
Water	207	10		80		537	338	132	227
B-factors									
Protein	90.14 $Å^2$	115.74 $Å^2$		67.52 $Å^2$		8.49 $Å^2$	9.37 $Å^2$	28.89 $Å^2$	20.87 $Å^2$
Hetatoms	112.89 $Å^2$			56.73 $Å^2$		24.45 $Å^2$	32.39 $Å^2$	35.06 $Å^2$	39.12 $Å^2$
Water	74.07 $Å^2$	81.05 $Å^2$		65.67 $Å^2$		22.45 $Å^2$	23.2 $Å^2$	35.26 $Å^2$	29.66 $Å^2$
r.m.s.d.									
Bond lengths	0.008 Å	0.01 Å		0.008 Å		0.016 Å	0.016 Å	0.015 Å	0.015 Å
Bond angles	0.89°	1.07°		1.25°		1.587°	1.336°	1.571°	1.661°
Protein Data Bank codes	4AP2	4APF		3I3N		2XN4	3II7	2VPJ	4ASC

[a] Values in parentheses are for the highest resolution shell.

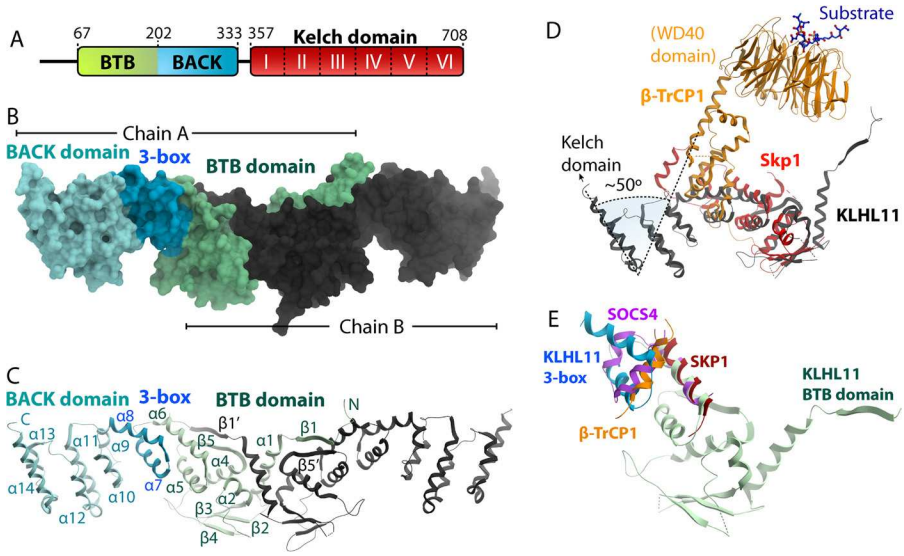

FIGURE 2. **Structure of the BTB-BACK domains of human KLHL11.** *A*, domain organization of human KLHL11. The domain boundaries of the BTB, BACK, and Kelch domains of KLHL11 are indicated, as well as the six Kelch repeats that constitute the complete Kelch domain. *B*, surface representation of the dimeric KLHL11 structure. Functional domains are color-coded in chain A, and chain B is colored *gray*. The 3-box includes the first two helices of the BACK domain. *C*, ribbon diagram of the of KLHL11 structure colored as in *B* and labeled by the convention of promyelocytic leukemia zinc finger protein (9). *D*, similar fold of the BTB domain and Skp1 was used for superposition of KLHL11 and the Skp1/β-TrCP1 complex (PDB code 1P22) (49). The BACK domain shows a different fold to the helical linker of β-TrCP1. *Dashed lines* mark the different orientations of the C-terminal helices that support the respective Kelch and WD40 β-propeller domains. *E*, superposition reveals that the 3-box of KLHL11 folds perpendicular to the analogous F-box of β-TrCP1 as well as the SOCS box of SOCS4 (PDB code 2IZV) (67).

18 Å wide between the BTB and BACK domains that exposes the 3-box for Cullin interaction (Fig. 2*B*).

Because the BTB-Kelch proteins are single chain analogs of other CRL substrate adaptors, such as Skp1/β-TrCP1, the BACK domain was expected to fold similarly to the F-box and helical linker regions of β-TrCP1 (15, 49). However, superposition of KLHL11 reveals a significant deviation from this arrangement (Fig. 2*D*). In particular, the long C-terminal helices that support the substrate-binding WD40 (β-TrCP1) or Kelch (KLHL11) domain show a 50° change in orientation (Fig. 2*D*). In part, this results from the distinct orientation of the 3-box, which packs perpendicular to the equivalent F-box or SOCS box motifs of other CRL substrate-recognition domains (Fig. 2*E*). These changes likely reflect the distinct architecture of the CRL3 class imposed by the BTB dimer.

Structural Diversity of the Kelch Substrate-Recognition Domain—The Kelch domain is the most widespread of the CRL3 substrate-recognition domains and recruits a diverse range of substrates. Structures are previously known only for the Kelch-like protein KEAP1 (KLHL19) (Fig. 3*A*) (22, 50, 51) and the Kelch-related protein KBTBD10 (KRP1) from *Rattus norvegicus* (52). To further characterize the diversity of these substrate-recognition domains, we determined the Kelch domain structures of the Kelch-like proteins KLHL2, KLHL7, and KLHL12, as well as the Kelch-related protein KBTBD5. All structures were refined at high resolution, ranging between 1.6 and 2.0 Å.

Although all four proteins display the typical β-propeller structure (Fig. 3*B*), there are systematic differences between KLHL and KBTBD proteins. The six Kelch repeats form the six "blades" of the propeller, each consisting of a four-stranded antiparallel β-sheet (Fig. 3*A*), with a C-terminal βA strand closing the propeller by completing blade I. This site shows divergence between the KLHL and KBTBD proteins. The Kelch-like (KLHL) proteins are characterized by consensus repeats, including a Gly-Gly pair that terminates strand βB, and hydrophobic Tyr (βC) and Trp (βD) residues that pack between blades (supplemental Fig. S1). In contrast, KBTBD5 exhibits an atypical repeat resulting in a more twisted blade I structure, as observed previously for KBTBD10 (52). Both KBTBD proteins also possess an extended C terminus that contributes a short βE strand to blade I as well as the usual βA (Fig. 3). Sequence comparisons suggest that this altered structure is a common feature of the KBTBD proteins (supplemental Fig. S1).

The surface properties of the six structures are strikingly diverse, reflecting their limited sequence identity. The substrate-binding site, first identified in the KEAP1-Nrf2 complex (51), lies on the narrower upper face of the Kelch domain (Fig. 3*A*). This surface displays a distinct electrostatic potential in each structure (Fig. 3*B*). The shape and size of the substrate pocket is determined by the inter-blade DA loops as well as the variable BC loops, which protrude significantly out of the upper propeller face (Fig. 3, *A* and *C*). Interestingly, KBTBD5 and KBTBD10 display a rather atypical loop arrangement, with an unusually short BC loop (three residues) in blade I flanked by greatly extended loops (18 and 20 residues, respectively) in blades II and VI (Fig. 3*C*). By contrast, the BC loops in the KLHL structures are more evenly distributed, with an average loop length of 12 residues. These variant features are expected to contribute to the precise substrate specificity of each BTB-Kelch family member.

Cul3 Binding to the 3-Box Involves a Specific N-terminal Extension Sequence—Substrate ubiquitylation requires the BTB-Kelch proteins to assemble with Cul3. To establish the molecular basis for Cul3 interaction, we adopted a split and express strategy for soluble protein expression (53). The Cul3

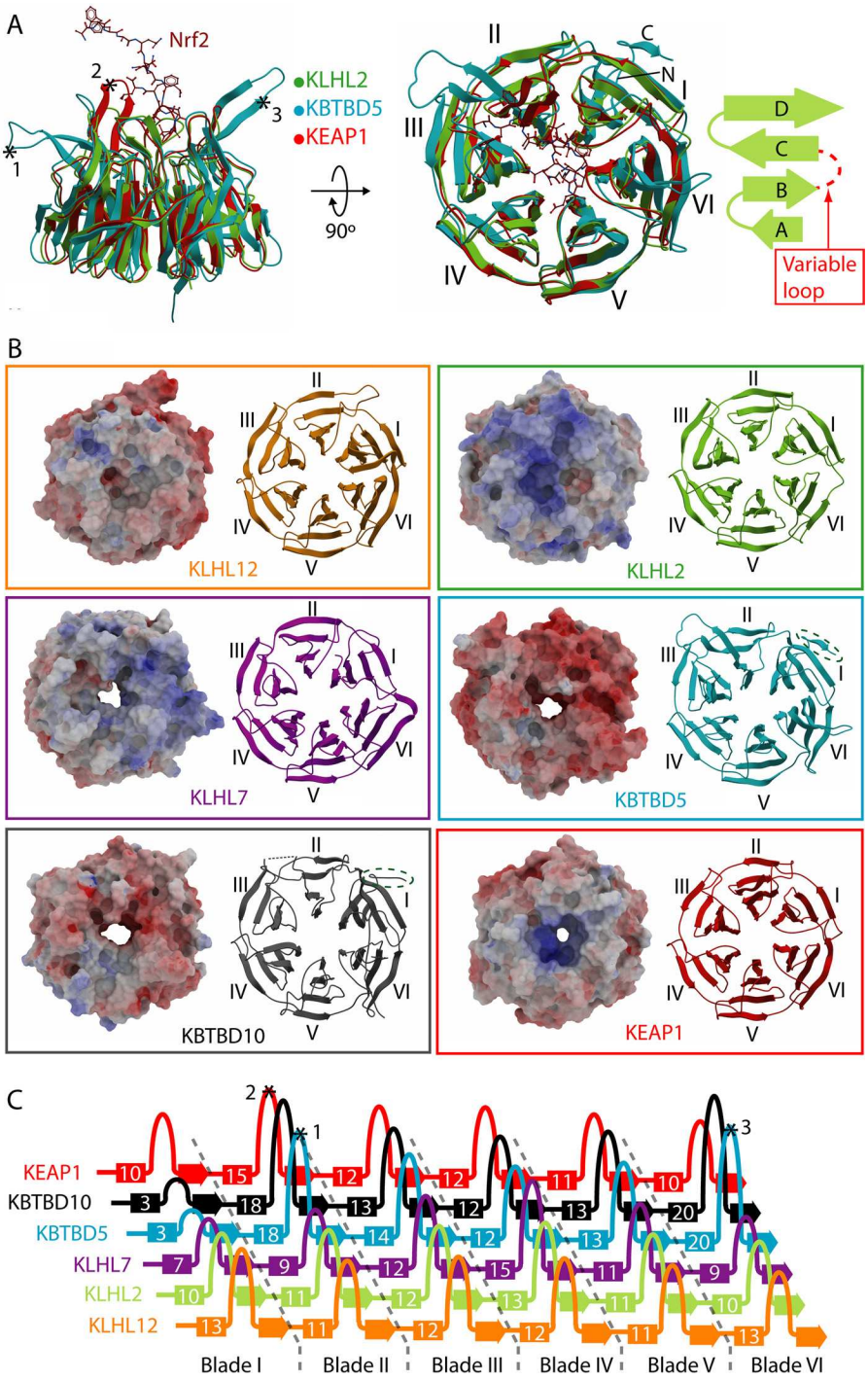

FIGURE 3. **Structural diversity of the Kelch domains.** *A*, superposition of the Kelch domains of KLHL2, KBTBD5, and the KEAP1-Nrf2 complex (PDB code 2FLU) (51). The six Kelch repeats, forming the "blades" of the β-propeller, are numbered *I–VI* from the N terminus. A schematic of one repeat shows the four constituent β-strands labeled *A–D* and the variable BC loop that contributes to substrate recognition. Three highly distinct BC loop conformations are marked *1–*3 in the ribbon diagram and similarly labeled in *C*. *B*, *ribbon* and surface representations of the Kelch domains of human KLHL2, KLHL7, KLHL12, and KBTBD5 as well as the previously solved structures of KEAP1 (PDB code 2FLU) and KBTBD10 (KRP1) from *R. norvegicus* (PDB code 2WOZ) (52). Electrostatic surface potentials are colored on a scale between −10 *kT/e* (*red*) and +10 *kT/e* (*blue*). A *dashed line* surrounds the unusual βE strand in the KBTBD proteins. *C*, schematic comparison of BC loop lengths across the six blades of each structure (lengths are indicated in *white*). Three loops marked in *A* are similarly labeled *1–*3 for reference.

NTD was subcloned with the solubilizing mutations I342R/L346D and co-purified with the previously characterized BTB-BACK domains of KLHL11. Crystals of the complex were first obtained in space group C2 using a Cul3 construct containing only the three consecutive Cullin-repeat domains ($Cul3_{NTD\Delta 22}$, Fig. 4*A*). Diffraction data were collected to 3.1-Å resolution, and the structure was solved by single isomorphous replacement with anomalous scattering (SIRAS) using a mercury derivative. The structural model indicated the potential for an unexpected interaction from the deleted Cul3 N-terminal extension. To address this, we identified a new crystal form in space group *I*121 containing the full $Cul3_{NTD}$ (Fig. 4*A*). The

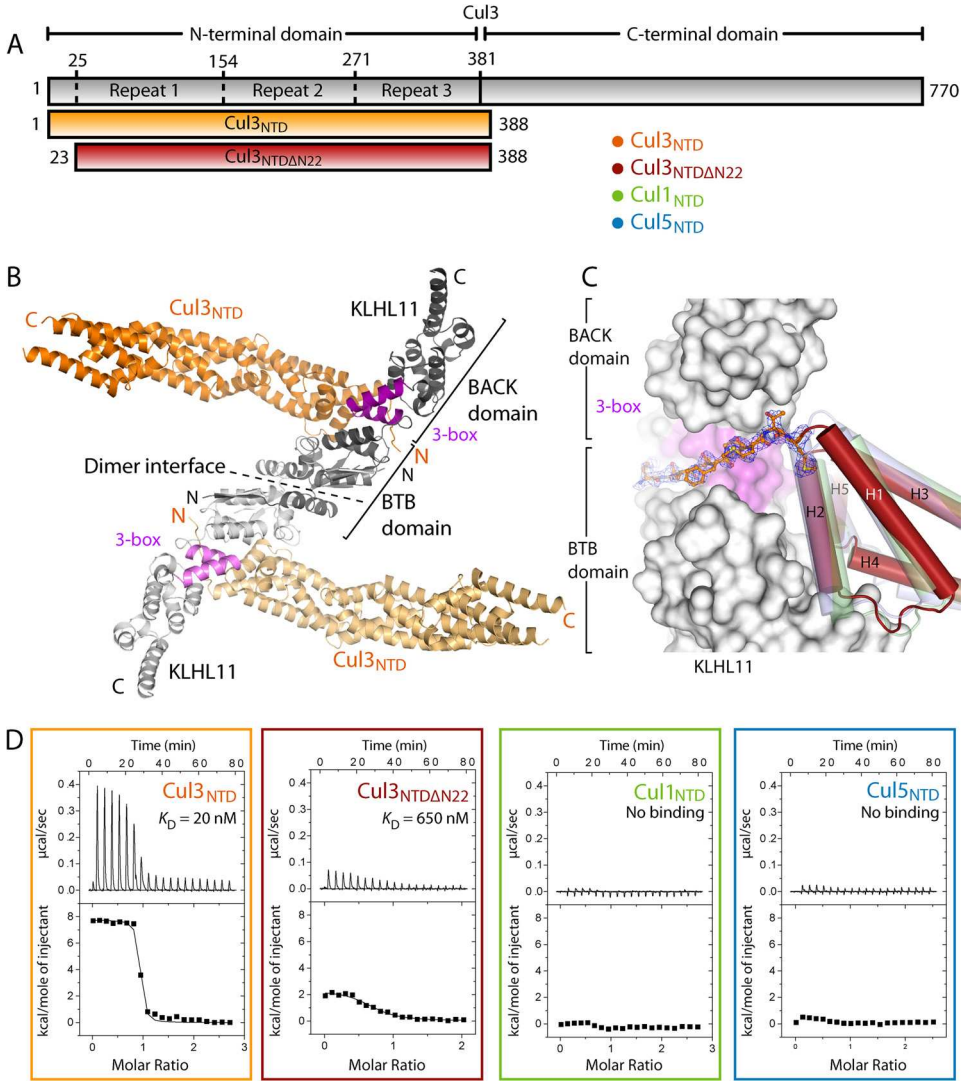

FIGURE 4. **Structure of the KLHL11-Cul3 complex.** *A*, domain organization of human Cul3 showing the domain boundaries of the N-terminal Cullin repeats and the C-terminal domain. The sequence coverage of the $Cul3_{NTD}$ and $Cul3_{NTD\Delta22}$ constructs used for crystallization and ITC is indicated below. *B*, *ribbon* representation of the human KLHL11-Cul3 structure highlighting different functional domains. *C*, surface representation of KLHL11 showing the interface with Cul3 (*cylinder* representation) as viewed from below with respect to *B*. Residues preceding Cul3 H1 (the N-terminal extension) bind the 3-box in a hydrophobic groove located between the BTB and BACK domains and are shown as *sticks* with the corresponding electron density ($2F_o - F_c$ map, contoured at 1σ) shown in *blue*. The structures of Cul1 (PDB code 1LDK) (7) and mouse Cul5 (PDB code 2WZK) are superimposed revealing the shorter H2 helix in Cul3. *D*, ITC measurements of the binding of KLHL11 to different human Cullin N-terminal domains demonstrating the absence of binding to non-Cul3 domains.

structure of this complex was solved using molecular replacement and refined at 2.8-Å resolution (Fig. 4*B*). Importantly, the electron density map allowed unambiguous tracing of a further eight N-terminal residues from Cul3 that packed in the hydrophobic groove located with the 3-box between the BTB and BACK domains of KLHL11 (Fig. 4*C*). An analogous groove was identified in the SCF complexes of Skp1 but was bound to an N-terminal sequence preceding the F-box (10, 49).

We were interested to assess the contribution of these Cul3 residues to the interaction and therefore measured the binding affinity of different Cullin proteins by ITC. $Cul3_{NTD\Delta22}$ containing only the Cullin-repeat domains bound KLHL11 relatively weakly (K_D = 0.65 μM, Fig. 4*D*). However, binding affinity was increased 30-fold upon inclusion of the Cul3 N-terminal extension ($Cul3_{NTD}$; K_D = 20 nM, Fig. 4*D*). As expected, there was essentially no binding of KLHL11 to the $Cul1_{NTD}$ or $Cul5_{NTD}$ (Fig. 4*D*), demonstrating the specificity of the interaction.

Structure of the KLHL11-Cul3 Complex—The two crystallized KLHL11-Cul3 complexes exhibited a 2-fold symmetry axis across the BTB dimer, resulting in only one KLHL11 and one Cul3 chain in each asymmetric unit. Generation of the symmetry-related molecules revealed the expected hetero-tetrameric assemblies, with each subunit in the KLHL11 homodimer binding one molecule of Cul3 (Fig. 4*B*). KLHL11 was clearly defined by electron density between residues 67 and 336 and the $Cul3_{NTD}$ between residues 17 and 381. Overall, the contact surface area of the $Cul3_{NTD}$ interface (1508 Å^2) was significantly larger than that of the $Cul3_{NTD\Delta22}$ complex (1018 Å^2), highlighting the importance of the N-terminal extension for Cul3 binding (Figs. 5, *A* and *B*, and 6*A*). By comparison, the SPOP-Cul3 structure (12), which lacks both the N-terminal

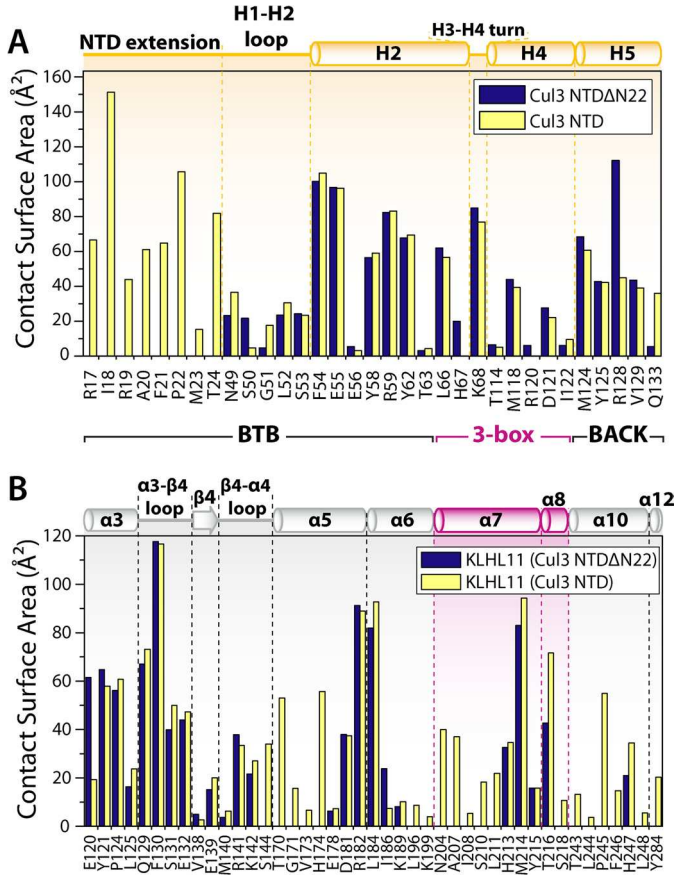

FIGURE 5. **N-terminal extension contributes significantly to the contact surface area.** *A*, residue-based surface areas of $Cul3_{NTD}$ and $Cul3_{NTD\Delta22}$ buried by KLHL11 interaction are shown as *bar graphs*. Values were calculated using the protein interfaces, surfaces, and assemblies service at the European Bioinformatics Institute (68). *B*, residue-based surface areas of KLHL11 buried by $Cul3_{NTD}$ and $Cul3_{NTD\Delta22}$, respectively, are shown as *bar graphs*.

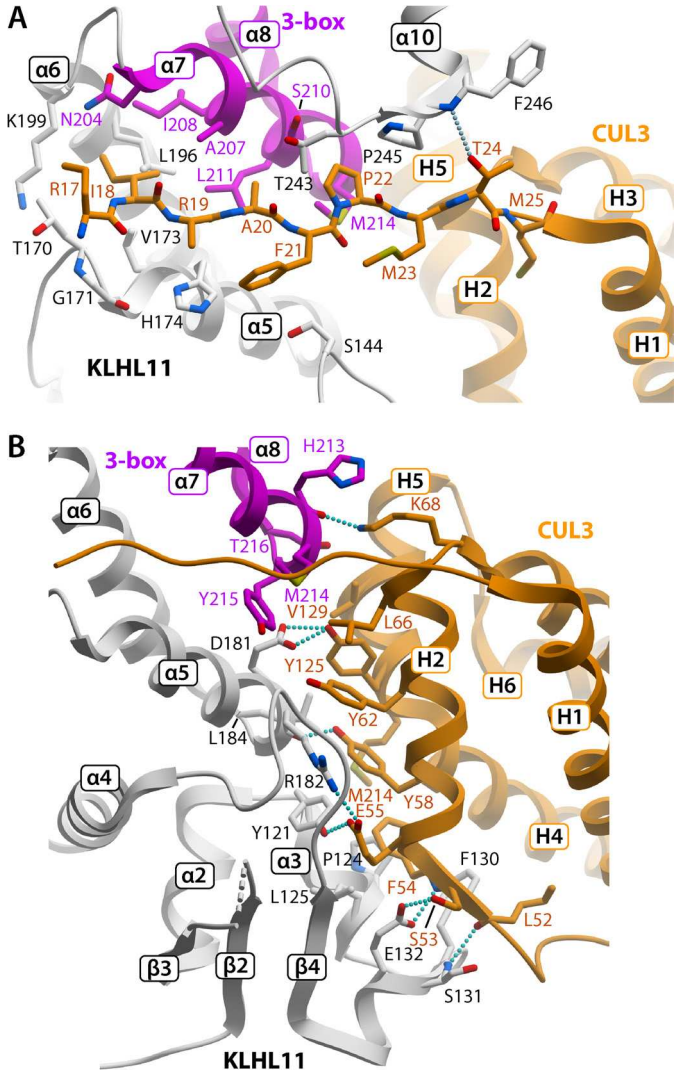

FIGURE 6. **Specific interactions in the KLHL11-Cul3 interface.** *A*, side chain interactions of the Cul3 N-terminal extension sequence in the hydrophobic groove of KLHL11. Intermolecular hydrogen bonds are shown by a *dashed blue line*. The side chains of Arg-17 and Arg-19 were not clearly defined in the electron density and were not built. View shown is the same as Fig. 4*C*. *B*, side chain interactions of the Cullin repeat domain with the BTB and 3-box domains of KLHL11 (same view as above).

extension and the 3-box/BACK domain, had a contact area of just 830 Å^2. Despite its stalk-like appearance, the Cul3 structure is remarkably conserved between the SPOP and KLHL11 complexes (0.8–1.3 Å root mean square deviation over 300 Cα atoms), suggesting that its conformation is relatively rigid.

The primary interface in the Cul3 complexes is formed by helices H2 and H5 of the first Cullin repeat, which pack against the BTB and 3-box domains of KLHL11 (Fig. 6*B*). Sequence conservation in the H2 and H5 helices is strong between Cul3 orthologs but weaker between paralogs (7). Furthermore, the H2 helix of Cul3 is a turn shorter than either Cul1 (7) or Cul5 (PDB code 2WZK) and therefore inserts comfortably into a shallow cleft in the BTB surface (Fig. 4*C*). In both KLHL11 and SPOP, this cleft forms via an induced fit mechanism facilitated by conformational changes in the α3-β4 loop (Fig. 7). This loop is disordered, or associated with higher crystallographic *B*-factors, in the unbound crystal structures but becomes helical upon Cul3 binding enabling hydrogen bonds from KLHL11 Ser-131 and Glu-132 to the Cul3 H2 helix (Figs. 6*B* and 7). In addition, Phe-130 (SPOP Met233) is shifted by some 5 Å to insert into a deep hydrophobic pocket formed between Cul3 helices H2 and H4 (Figs. 6*B* and 7).

The KLHL11 complex reveals for the first time how the 3-box binds to Cul3. The motif, including KLHL11 α7 and α8, contributes both to the interface with the first Cullin repeat (Fig. 6*B*) and to the hydrophobic groove that accommodates the Cul3 N-terminal extension sequence (Fig. 6*A*). The Cullin-repeat interaction is mediated largely by the 3-box α7-α8 loop that packs against the C-terminal regions of Cul3 H2 and H5 (Fig. 6*B*). Here, the backbone carbonyl of KLHL11 His-213 (α7) forms a single hydrogen bond with Cul3 Lys-68. The Cul3 N-terminal extension sequence runs antiparallel to the 3-box α7 helix and is flanked by the α5/α6 and α9/α10 helices of the BTB and BACK domains, respectively (Fig. 6*A*). A single hydrogen bond is formed from the side chain oxygen of Cul3 Thr-24 to the backbone nitrogen of KLHL11 Phe-246 (α10). The remaining N-terminal Cul3 contacts are hydrophobic. In particular, the side chains of Cul3 Ile-18, Ala-20, and Pro-22 insert directly into the hydrophobic groove of KLHL11 to contribute substantially to the overall contact area (Fig. 5*A*).

Model for the Dimeric CRL3 Complex—The KLHL11-Cul3 structure establishes the core architecture of the dimeric BTB-

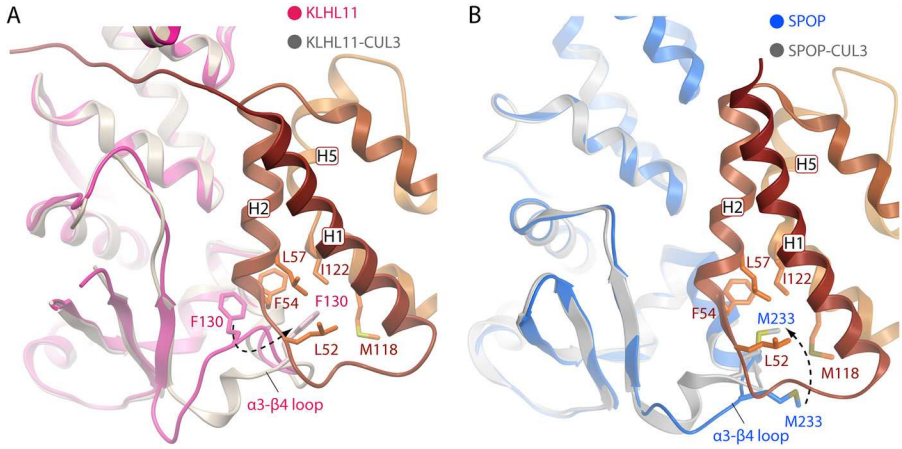

FIGURE 7. **Conserved assembly of SPOP-Cul3 and KLHL11-Cul3 complexes.** *A*, superposition of the unbound (*magenta*) and bound (*gray*) KLHL11 structures highlighting the conformational change of the α3–β4 loop upon association with Cul3 (*orange*). A *dashed arrow* indicates a 5-Å movement of KLHL11 Phe-130. *B*, superposition of the unbound and bound SPOP structures highlights a similar conformational change of the α3-β4 loop upon association with Cul3. A *dashed arrow* indicates the movement of Met-233 (equivalent to KLHL11 Phe-130).

Kelch class of E3 ligase. To generate a working model of the complete E3, we built the missing structural domains using other available structures. The $Cul3_{CTD}$ was built initially from the Cul1 structure (PDB 1LDK) (7) and then modified to fit the active conformation of the neddylated $Cul5_{CTD}$-Rbx1 complex (PDB 3DQV) (5). An E2-ubiquitin intermediate was modeled from the UbcH5A-ubiquitin structure (PDB 4AP4) (54) and docked onto Rbx1 by its homology to the Cbl-UbcH7 complex (PDB 1FBV) (55). Finally, the Kelch domain and substrate from the KEAP1-Nrf2 complex (PDB 2FLU) (51) were modeled atop helix α14 of the BACK domain of KLHL11. The final model places the two E2-ubiquitin intermediates at the center of the complex where they dissect the axis between the two Kelch domains (Fig. 8*A*). Flexibility in the linker between the BACK and Kelch domains as well as the limited freedom of the RING domain of Rbx1 may help to bridge the substrate-ubiquitin gap and to break the overall symmetry specified by KLHL11.

DISCUSSION

Here, we show that the interaction of Cul3 with the BTB-Kelch family is unexpectedly two parts. In addition to the expected Cullin-repeat-BTB interaction, we define a novel interaction between the specific N-terminal extension sequence of Cul3 and the 3-box of KLHL11. Previously, the interaction of an N-terminal extension sequence was considered unique to Cul4 (56, 57). The surprise interaction of the Cul3 N-terminal region is facilitated by a proximal hydrophobic groove located at the interface of the BTB, 3-box, and BACK domains. Occupying this site enables the N-terminal extension to form contacts across all three KLHL11 domains and therefore to contribute significantly to the overall binding affinity. Notably, the bound Cullin-repeat is also enveloped by the BTB α3-β4 loop that refolds around the relatively short H2 helix like a molecular clamp. A similar BTB adaptor interface is found in the SPOP-Cul3 complex (12) suggesting that this is indeed a conserved mechanism of Cul3 interaction.

Upon assembly with Cul3, the BTB-Kelch proteins may direct dynamic control of ubiquitylation through the bivalent coordination of a single substrate molecule. A "fixed-ends"

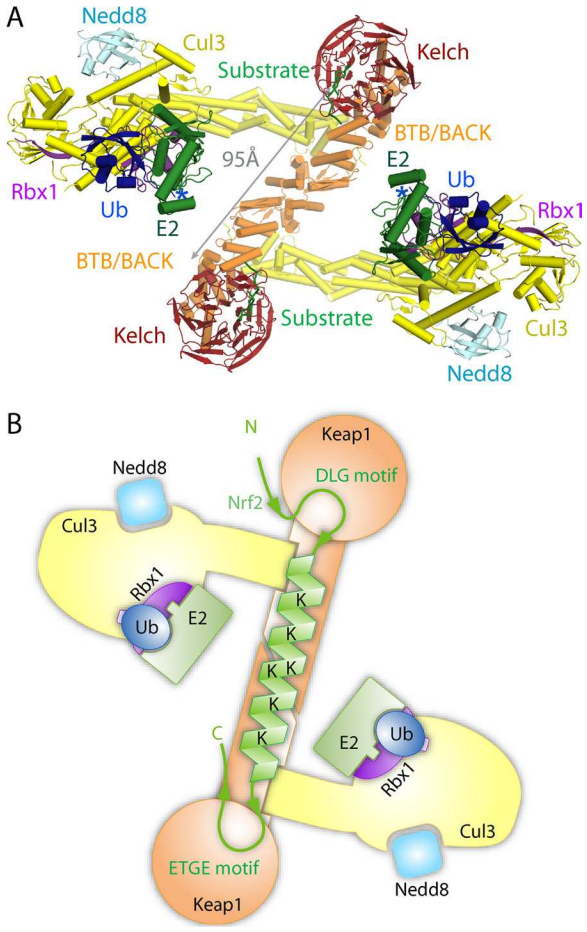

FIGURE 8. **Model of an active BTB-Kelch E3 ligase.** *A*, model of a complete BTB-Kelch E3 ligase complex was constructed using the core architecture defined by the KLHL11-Cul3 complex. Missing structural domains were modeled from other available structures, including PDB codes 1LDK and 3DQV for the Cullin CTD-Rbx1-Nedd8 complex, 1FBV and 4AP4 for the E2-ubiquitin intermediate, and 2FLU for the Kelch-substrate complex. *Asterisks* mark the positions of the reactive E2-ubiquitin (*Ub*) thioester bonds. *B*, schematic representation of the two-site recognition model proposed for Nrf2 recruitment by KEAP1. The intervening α-helix contains seven substrate lysines of which six are predicted to fall on the same face (18).

model is proposed for Nrf2 recruitment in which high (ETGE) and low (DLG) affinity recognition motifs are tethered to the two Kelch domains of a KEAP1 homodimer to promote ubiquitylation of a central lysine-rich α-helix (18–21). The presented structures offer a molecular model to support this hypothesis (Fig. 8*B*). The elongated BTB-BACK domains establish a spacer suitable for Nrf2 recruitment while orienting the associated Cullin-RING complexes to position the E2 molecules centrally for ubiquitin transfer. The architecture of the KEAP1 protein has also been determined by single particle electron microscopy (EM) (20). Consistent with this study, the reconstruction at 24 Å resolution revealed an elongated structure with a 2-fold symmetry axis. Two distinct globular domains were attached by short linker arms to a central stem. The crystal structures indicate that the linker likely corresponds to the 3-box that separates the BTB stem from the globular domains, each comprising a Kelch domain atop the BACK domain helices α9–α14. In the EM reconstruction, the positions of the two substrate-binding sites were somewhat flexible with an average separation of 80 Å (20). Some 47 residues separate the ETGE and DLG motifs, giving a theoretic span of 98 Å, assuming a 33-residue helix (18). Our structural model provides a span of 95 Å, broadly consistent with the EM data.

Dimerization is also required for the E3 activity of some SCF complexes, including those of β-TrCP1 and Cdc4 (58). In contrast to the BTB adaptors, these CRL1 complexes dimerize through the D domain of the substrate-recognition module (58). Their predicted assemblies also position the substrate centrally to two catalytic centers, although a distinct configuration is enforced due to the alternative mode of dimerization. In addition to robust substrate capture, dimeric E3s may confer greater spatial variability to enable efficient ubiquitylation of diverse substrate lysine acceptor sites. E3 interaction is also thought to bias dynamic E2-ubiquitin ensembles toward a conformation with enhanced reactivity for substrate lysines. In some E3 classes, this reaction is catalyzed by dimerization of the RING domain (54, 59, 60), although it remains unclear how this mechanism could be utilized by the CRL families. Given the relative positions of the Rbx1 subunits in the structural model, such a mechanism would likely require higher order CRL3 assembly, as suggested for the MATH-BTB protein SPOP (12).

Uniquely, the BTB-Kelch family proteins integrate the functions of both CRL adaptors and substrate receptors. Cul3 must therefore assemble with a large number of distinct BTB adaptor domains, whereas other Cullins bind a common adaptor protein such as Skp1 or ElonginC. As a consequence, BTB E3 ligases may offer a greater diversity of drug-targeting sites for investigation. In this respect, several sites in the KLHL11 structure are of interest, including the BTB-dimer interface, the Cullin-repeat interface, and the hydrophobic groove of the 3-box. Indeed, disruption of Cul3 N-terminal interactions with the hydrophobic groove resulted in a 30-fold loss in affinity. A similar decrease was observed upon deletion of the 3-box in SPOP (30). Promisingly, small molecules have been identified previously that target the corepressor binding groove of the BCL6 BTB domain (61) as well as the substrate binding grooves of E3 ligases, including MDM2 (62), VHL (63), and Skp2 (64).

The presented structures reveal the novel architecture of BTB-Cul3 assembly and impact our mechanistic understanding of CRL3 activity with potential therapeutic implications.

Acknowledgments—We thank the staff at Diamond Light Source and the Swiss Light Source for assistance with data collection experiments.

REFERENCES

1. Schulman, B. A., and Harper, J. W. (2009) Ubiquitin-like protein activation by E1 enzymes: the apex for downstream signaling pathways. *Nat. Rev. Mol. Cell Biol.* **10,** 319–331
2. Hershko, A., and Ciechanover, A. (1998) The ubiquitin system. *Annu. Rev. Biochem.* **67,** 425–479
3. Petroski, M. D., and Deshaies, R. J. (2005) Function and regulation of cullin-RING ubiquitin ligases. *Nat. Rev. Mol. Cell Biol.* **6,** 9–20
4. Zimmerman, E. S., Schulman, B. A., and Zheng, N. (2010) Structural assembly of cullin-RING ubiquitin ligase complexes. *Curr. Opin. Struct. Biol.* **20,** 714–721
5. Duda, D. M., Borg, L. A., Scott, D. C., Hunt, H. W., Hammel, M., and Schulman, B. A. (2008) Structural insights into NEDD8 activation of cullin-RING ligases: conformational control of conjugation. *Cell* **134,** 995–1006
6. Saha, A., and Deshaies, R. J. (2008) Multimodal activation of the ubiquitin ligase SCF by Nedd8 conjugation. *Mol. Cell* **32,** 21–31
7. Zheng, N., Schulman, B. A., Song, L., Miller, J. J., Jeffrey, P. D., Wang, P., Chu, C., Koepp, D. M., Elledge, S. J., Pagano, M., Conaway, R. C., Conaway, J. W., Harper, J. W., and Pavletich, N. P. (2002) Structure of the Cul1-Rbx1-Skp1-F boxSkp2 SCF ubiquitin ligase complex. *Nature* **416,** 703–709
8. Pintard, L., Willems, A., and Peter, M. (2004) Cullin-based ubiquitin ligases: Cul3-BTB complexes join the family. *EMBO J.* **23,** 1681–1687
9. Ahmad, K. F., Engel, C. K., and Privé, G. G. (1998) Crystal structure of the BTB domain from PLZF. *Proc. Natl. Acad. Sci. U.S.A.* **95,** 12123–12128
10. Schulman, B. A., Carrano, A. C., Jeffrey, P. D., Bowen, Z., Kinnucan, E. R., Finnin, M. S., Elledge, S. J., Harper, J. W., Pagano, M., and Pavletich, N. P. (2000) Insights into SCF ubiquitin ligases from the structure of the Skp1-Skp2 complex. *Nature* **408,** 381–386
11. Stebbins, C. E., Kaelin, W. G., Jr., and Pavletich, N. P. (1999) Structure of the VHL-ElonginC-ElonginB complex: implications for VHL tumor suppressor function. *Science* **284,** 455–461
12. Errington, W. J., Khan, M. Q., Bueler, S. A., Rubinstein, J. L., Chakrabartty, A., and Privé, G. G. (2012) Adaptor protein self-assembly drives the control of a cullin-RING ubiquitin ligase. *Structure* **20,** 1141–1153
13. Stogios, P. J., Downs, G. S., Jauhal, J. J., Nandra, S. K., and Privé, G. G. (2005) Sequence and structural analysis of BTB domain proteins. *Genome Biol.* **6,** R82
14. Prag, S., and Adams, J. C. (2003) Molecular phylogeny of the kelch-repeat superfamily reveals an expansion of BTB/kelch proteins in animals. *BMC Bioinformatics* **4,** 42
15. Stogios, P. J., and Privé, G. G. (2004) The BACK domain in BTB-kelch proteins. *Trends Biochem. Sci.* **29,** 634–637
16. McMahon, M., Itoh, K., Yamamoto, M., and Hayes, J. D. (2003) Keap1-dependent proteasomal degradation of transcription factor Nrf2 contributes to the negative regulation of antioxidant response element-driven gene expression. *J. Biol. Chem.* **278,** 21592–21600
17. Kobayashi, A., Kang, M. I., Okawa, H., Ohtsuji, M., Zenke, Y., Chiba, T., Igarashi, K., and Yamamoto, M. (2004) Oxidative stress sensor Keap1 functions as an adaptor for Cul3-based E3 ligase to regulate proteasomal degradation of Nrf2. *Mol. Cell. Biol.* **24,** 7130–7139
18. Tong, K. I., Katoh, Y., Kusunoki, H., Itoh, K., Tanaka, T., and Yamamoto, M. (2006) Keap1 recruits Neh2 through binding to ETGE and DLG motifs: characterization of the two-site molecular recognition model. *Mol. Cell. Biol.* **26,** 2887–2900
19. Tong, K. I., Padmanabhan, B., Kobayashi, A., Shang, C., Hirotsu, Y., Yokoyama, S., and Yamamoto, M. (2007) Different electrostatic potentials define ETGE and DLG motifs as hinge and latch in oxidative stress re-

sponse. *Mol. Cell. Biol.* **27,** 7511–7521
20. Ogura, T., Tong, K. I., Mio, K., Maruyama, Y., Kurokawa, H., Sato, C., and Yamamoto, M. (2010) Keap1 is a forked-stem dimer structure with two large spheres enclosing the intervening, double glycine repeat, and C-terminal domains. *Proc. Natl. Acad. Sci. U.S.A.* **107,** 2842–2847
21. McMahon, M., Thomas, N., Itoh, K., Yamamoto, M., and Hayes, J. D. (2006) Dimerization of substrate adaptors can facilitate cullin-mediated ubiquitylation of proteins by a "tethering" mechanism: a two-site interaction model for the Nrf2-Keap1 complex. *J. Biol. Chem.* **281,** 24756–24768
22. Padmanabhan, B., Tong, K. I., Ohta, T., Nakamura, Y., Scharlock, M., Ohtsuji, M., Kang, M. I., Kobayashi, A., Yokoyama, S., and Yamamoto, M. (2006) Structural basis for defects of Keap1 activity provoked by its point mutations in lung cancer. *Mol. Cell* **21,** 689–700
23. Singh, A., Misra, V., Thimmulappa, R. K., Lee, H., Ames, S., Hoque, M. O., Herman, J. G., Baylin, S. B., Sidransky, D., Gabrielson, E., Brock, M. V., and Biswal, S. (2006) Dysfunctional KEAP1-NRF2 interaction in non-small-cell lung cancer. *PLoS Med.* **3,** e420
24. Boyden, L. M., Choi, M., Choate, K. A., Nelson-Williams, C. J., Farhi, A., Toka, H. R., Tikhonova, I. R., Bjornson, R., Mane, S. M., Colussi, G., Lebel, M., Gordon, R. D., Semmekrot, B. A., Poujol, A., Välimäki, M. J., De Ferrari, M. E., Sanjad, S. A., Gutkin, M., Karet, F. E., Tucci, J. R., Stockigt, J. R., Keppler-Noreuil, K. M., Porter, C. C., Anand, S. K., Whiteford, M. L., Davis, I. D., Dewar, S. B., Bettinelli, A., Fadrowski, J. J., Belsha, C. W., Hunley, T. E., Nelson, R. D., Trachtman, H., Cole, T. R., Pinsk, M., Bockenhauer, D., Shenoy, M., Vaidyanathan, P., Foreman, J. W., Rasoulpour, M., Thameem, F., Al-Shahrouri, H. Z., Radhakrishnan, J., Gharavi, A. G., Goilav, B., and Lifton, R. P. (2012) Mutations in kelch-like 3 and cullin 3 cause hypertension and electrolyte abnormalities. *Nature* **482,** 98–102
25. Friedman, J. S., Ray, J. W., Waseem, N., Johnson, K., Brooks, M. J., Hugosson, T., Breuer, D., Branham, K. E., Krauth, D. S., Bowne, S. J., Sullivan, L. S., Ponjavic, V., Gränse, L., Khanna, R., Trager, E. H., Gieser, L. M., Hughbanks-Wheaton, D., Cojocaru, R. I., Ghiasvand, N. M., Chakarova, C. F., Abrahamson, M., Göring, H. H., Webster, A. R., Birch, D. G., Abecasis, G. R., Fann, Y., Bhattacharya, S. S., Daiger, S. P., Heckenlively, J. R., Andréasson, S., and Swaroop, A. (2009) Mutations in a BTB-Kelch protein, KLHL7, cause autosomal-dominant retinitis pigmentosa. *Am. J. Hum. Genet.* **84,** 792–800
26. Cirak, S., von Deimling, F., Sachdev, S., Errington, W. J., Herrmann, R., Bönnemann, C., Brockmann, K., Hinderlich, S., Lindner, T. H., Steinbrecher, A., Hoffmann, K., Privé, G. G., Hannink, M., Nürnberg, P., and Voit, T. (2010) Kelch-like homologue 9 mutation is associated with an early onset autosomal dominant distal myopathy. *Brain* **133,** 2123–2135
27. Jin, L., Pahuja, K. B., Wickliffe, K. E., Gorur, A., Baumgärtel, C., Schekman, R., and Rape, M. (2012) Ubiquitin-dependent regulation of COPII coat size and function. *Nature* **482,** 495–500
28. Rondou, P., Haegeman, G., Vanhoenacker, P., and Van Craenenbroeck, K. (2008) BTB Protein KLHL12 targets the dopamine D4 receptor for ubiquitination by a Cul3-based E3 ligase. *J. Biol. Chem.* **283,** 11083–11096
29. Angers, S., Thorpe, C. J., Biechele, T. L., Goldenberg, S. J., Zheng, N., MacCoss, M. J., and Moon, R. T. (2006) The KLHL12-Cullin-3 ubiquitin ligase negatively regulates the Wnt-β-catenin pathway by targeting Dishevelled for degradation. *Nat. Cell Biol.* **8,** 348–357
30. Zhuang, M., Calabrese, M. F., Liu, J., Waddell, M. B., Nourse, A., Hammel, M., Miller, D. J., Walden, H., Duda, D. M., Seyedin, S. N., Hoggard, T., Harper, J. W., White, K. P., and Schulman, B. A. (2009) Structures of SPOP-substrate complexes: insights into molecular architectures of BTB-Cul3 ubiquitin ligases. *Mol. Cell* **36,** 39–50
31. Savitsky, P., Bray, J., Cooper, C. D., Marsden, B. D., Mahajan, P., Burgess-Brown, N. A., and Gileadi, O. (2010) High-throughput production of human proteins for crystallization: the SGC experience. *J. Struct. Biol.* **172,** 3–13
32. Leslie, A. G., and Powell, H. R. (2007) in *Evolving Methods for Macromolecular Crystallography* (Read, R. J., and Sussman, J. L., eds) pp. 41–51, Springer, Netherlands
33. Kabsch, W. (2010) XDS. *Acta Crystallogr. D Biol. Crystallogr.* **66,** 125–132
34. Evans, P. (2006) Scaling and assessment of data quality. *Acta Crystallogr. D Biol. Crystallogr.* **62,** 72–82
35. Collaborative Computational Project No. 4 (1994) The CCP4 suite: programs for protein crystallography. *Acta Crystallogr. D Biol. Crystallogr.* **50,** 760–763
36. Vonrhein, C., Blanc, E., Roversi, P., and Bricogne, G. (2007) Automated structure solution with autoSHARP. *Methods Mol. Biol.* **364,** 215–230
37. McCoy, A. J., Grosse-Kunstleve, R. W., Adams, P. D., Winn, M. D., Storoni, L. C., and Read, R. J. (2007) Phaser crystallographic software. *J. Appl. Crystallogr.* **40,** 658–674
38. Cowtan, K. (2010) Recent developments in classical density modification. *Acta Crystallogr. D Biol. Crystallogr.* **66,** 470–478
39. Cowtan, K. (2008) Fitting molecular fragments into electron density. *Acta Crystallogr. D Biol. Crystallogr.* **64,** 83–89
40. Cowtan, K. (2006) The Buccaneer software for automated model building. 1. Tracing protein chains. *Acta Crystallogr. D Biol. Crystallogr.* **62,** 1002–1011
41. Adams, P. D., Afonine, P. V., Bunkóczi, G., Chen, V. B., Davis, I. W., Echols, N., Headd, J. J., Hung, L. W., Kapral, G. J., Grosse-Kunstleve, R. W., McCoy, A. J., Moriarty, N. W., Oeffner, R., Read, R. J., Richardson, D. C., Richardson, J. S., Terwilliger, T. C., and Zwart, P. H. (2010) PHENIX: a comprehensive Python-based system for macromolecular structure solution. *Acta Crystallogr. D Biol. Crystallogr.* **66,** 213–221
42. Emsley, P., Lohkamp, B., Scott, W. G., and Cowtan, K. (2010) Features and development of Coot. *Acta Crystallogr. D Biol. Crystallogr.* **66,** 486–501
43. Brünger, A. T., Adams, P. D., Clore, G. M., DeLano, W. L., Gros, P., Grosse-Kunstleve, R. W., Jiang, J. S., Kuszewski, J., Nilges, M., Pannu, N. S., Read, R. J., Rice, L. M., Simonson, T., and Warren, G. L. (1998) Crystallography & NMR system: A new software suite for macromolecular structure determination. *Acta Crystallogr. D Biol. Crystallogr.* **54,** 905–921
44. Brunger, A. T. (2007) Version 1.2 of the crystallography and NMR system. *Nat. Protoc.* **2,** 2728–2733
45. Murshudov, G. N., Vagin, A. A., and Dodson, E. J. (1997) Refinement of macromolecular structures by the maximum-likelihood method. *Acta Crystallogr. D Biol. Crystallogr.* **53,** 240–255
46. Murshudov, G. N., Skubák, P., Lebedev, A. A., Pannu, N. S., Steiner, R. A., Nicholls, R. A., Winn, M. D., Long, F., and Vagin, A. A. (2011) REFMAC5 for the refinement of macromolecular crystal structures. *Acta Crystallogr. D Biol. Crystallogr.* **67,** 355–367
47. Bricogne, G., Blanc, E., Brandl, M., Flensburg, C., Keller, P., Paciorek, W., Roversi, P., Sharff, A., Smart, O. S., Vonrhein, C., and Womack, T. O. (2011) *BUSTER*, Version 2.10.0 Ed., Global Phasing Ltd., Cambridge, UK
48. Chen, V. B., Arendall, W. B., 3rd, Headd, J. J., Keedy, D. A., Immormino, R. M., Kapral, G. J., Murray, L. W., Richardson, J. S., and Richardson, D. C. (2010) MolProbity: all-atom structure validation for macromolecular crystallography. *Acta Crystallogr. D Biol. Crystallogr.* **66,** 12–21
49. Wu, G., Xu, G., Schulman, B. A., Jeffrey, P. D., Harper, J. W., and Pavletich, N. P. (2003) Structure of a β-TrCP1-Skp1-β-catenin complex: destruction motif binding and lysine specificity of the SCF(β-TrCP1) ubiquitin ligase. *Mol. Cell* **11,** 1445–1456
50. Li, X., Zhang, D., Hannink, M., and Beamer, L. J. (2004) Crystal structure of the Kelch domain of human Keap1. *J. Biol. Chem.* **279,** 54750–54758
51. Lo, S. C., Li, X., Henzl, M. T., Beamer, L. J., and Hannink, M. (2006) Structure of the Keap1:Nrf2 interface provides mechanistic insight into Nrf2 signaling. *EMBO J.* **25,** 3605–3617
52. Gray, C. H., McGarry, L. C., Spence, H. J., Riboldi-Tunnicliffe, A., and Ozanne, B. W. (2009) Novel β-propeller of the BTB-Kelch protein Krp1 provides a binding site for Lasp-1 that is necessary for pseudopodial extension. *J. Biol. Chem.* **284,** 30498–30507
53. Li, T., Pavletich, N. P., Schulman, B. A., and Zheng, N. (2005) High level expression and purification of recombinant SCF ubiquitin ligases. *Methods Enzymol.* **398,** 125–142
54. Plechanovová, A., Jaffray, E. G., Tatham, M. H., Naismith, J. H., and Hay, R. T. (2012) Structure of a RING E3 ligase and ubiquitin-loaded E2 primed for catalysis. *Nature* **489,** 115–120
55. Zheng, N., Wang, P., Jeffrey, P. D., and Pavletich, N. P. (2000) Structure of a c-Cbl-UbcH7 complex: RING domain function in ubiquitin-protein ligases. *Cell* **102,** 533–539
56. Angers, S., Li, T., Yi, X., MacCoss, M. J., Moon, R. T., and Zheng, N. (2006) Molecular architecture and assembly of the DDB1-CUL4A ubiquitin ligase machinery. *Nature* **443,** 590–593

57. Fischer, E. S., Scrima, A., Böhm, K., Matsumoto, S., Lingaraju, G. M., Faty, M., Yasuda, T., Cavadini, S., Wakasugi, M., Hanaoka, F., Iwai, S., Gut, H., Sugasawa, K., and Thomä, N. H. (2011) The molecular basis of CRL4DDB2/CSA ubiquitin ligase architecture, targeting, and activation. *Cell* **147,** 1024–1039
58. Tang, X., Orlicky, S., Lin, Z., Willems, A., Neculai, D., Ceccarelli, D., Mercurio, F., Shilton, B. H., Sicheri, F., and Tyers, M. (2007) Suprafacial orientation of the SCFCdc4 dimer accommodates multiple geometries for substrate ubiquitination. *Cell* **129,** 1165–1176
59. Dou, H., Buetow, L., Sibbet, G. J., Cameron, K., and Huang, D. T. (2012) BIRC7-E2 ubiquitin conjugate structure reveals the mechanism of ubiquitin transfer by a RING dimer. *Nat. Struct. Mol. Biol.* **19,** 876–883
60. Pruneda, J. N., Littlefield, P. J., Soss, S. E., Nordquist, K. A., Chazin, W. J., Brzovic, P. S., and Klevit, R. E. (2012) Structure of an E3:E2~Ub complex reveals an allosteric mechanism shared among RING/U-box ligases. *Mol. Cell* **47,** 933–942
61. Cerchietti, L. C., Ghetu, A. F., Zhu, X., Da Silva, G. F., Zhong, S., Matthews, M., Bunting, K. L., Polo, J. M., Farès, C., Arrowsmith, C. H., Yang, S. N., Garcia, M., Coop, A., Mackerell, A. D., Jr., Privé, G. G., and Melnick, A. (2010) A small-molecule inhibitor of BCL6 kills DLBCL cells *in vitro* and *in vivo*. *Cancer Cell* **17,** 400–411
62. Vassilev, L. T., Vu, B. T., Graves, B., Carvajal, D., Podlaski, F., Filipovic, Z., Kong, N., Kammlott, U., Lukacs, C., Klein, C., Fotouhi, N., and Liu, E. A. (2004) *In vivo* activation of the p53 pathway by small-molecule antagonists of MDM2. *Science* **303,** 844–848
63. Buckley, D. L., Gustafson, J. L., Van Molle, I., Roth, A. G., Tae, H. S., Gareiss, P. C., Jorgensen, W. L., Ciulli, A., and Crews, C. M. (2012) Small-molecule inhibitors of the interaction between the E3 Ligase VHL and HIF1α. *Angew. Chem. Int. Ed. Engl.* **51,** 11463–11467
64. Wu, L., Grigoryan, A. V., Li, Y., Hao, B., Pagano, M., and Cardozo, T. J. (2012) Specific small molecule inhibitors of Skp2-mediated p27 degradation. *Chem. Biol.* **19,** 1515–1524
65. Chenna, R., Sugawara, H., Koike, T., Lopez, R., Gibson, T. J., Higgins, D. G., and Thompson, J. D. (2003) Multiple sequence alignment with the Clustal series of programs. *Nucleic Acids Res.* **31,** 3497–3500
66. Choi, J. H., Jung, H. Y., Kim, H. S., and Cho, H. G. (2000) PhyloDraw: a phylogenetic tree drawing system. *Bioinformatics* **16,** 1056–1058
67. Bullock, A. N., Rodriguez, M. C., Debreczeni, J. E., Songyang, Z., and Knapp, S. (2007) Structure of the SOCS4-ElonginB/C complex reveals a distinct SOCS box interface and the molecular basis for SOCS-dependent EGFR degradation. *Structure* **15,** 1493–1504
68. Krissinel, E., and Henrick, K. (2007) Inference of macromolecular assemblies from crystalline state. *J. Mol. Biol.* **372,** 774–797